

## **MULTI-MODE HORN DESIGN AND BEAM CHARACTERISTICS FOR PLANCK**

J.A. Murphy<sup>1</sup>, T. Peacocke<sup>1</sup>, B. Maffei<sup>2</sup>, I. McAuley<sup>1</sup>, F. Noviello<sup>1,3</sup>, V. Yurchenko<sup>1,10</sup>, P.A.R. Ade<sup>4</sup>, G. Savini<sup>9,4</sup>, J-M. Lamarre<sup>5</sup>, J. Brossard<sup>6,7</sup>, R. Colgan<sup>1</sup>, E. Gleeson<sup>1</sup>, A.E. Lange<sup>8</sup>, Y. Longval<sup>3</sup>, G. Pisano<sup>2</sup>, J-L. Puget<sup>3</sup>, I. Ristorcelli<sup>6</sup>, R. Sudiwala<sup>4,8</sup> and R.J. Wylde<sup>11</sup>

1 NUI Maynooth, Department of Experimental Physics, Maynooth, Co. Kildare, Ireland

2 The University of Manchester, JBCA, School of Physics and Astronomy, Manchester M13 9PL, UK

e-mail: Bruno.maffei@manchester.ac.uk

3 Institut d'Astrophysique Spatiale, Université Paris 11, Batiment 121, 91405 Orsay, France

4 Cardiff University, School of Physics and Astronomy, The Parade, Cardiff CF24 3AA, UK

5 LERMA, Observatoire de Paris, 61 Avenue de l'Observatoire, 75014 Paris, France

6 CESR, CNRS-Université, 9 av. du colonel Roche, BP44346, 31038 Toulouse Cedex 4, France

7 LAL, Université Paris-Sud 11, Batiment 200, 91898 Orsay, France

8 Caltech/JPL, Caltech Observational Cosmology, Mail code:59-33, Pasadena, CA 91125, USA

9 Optical Science Laboratory, Dept. of Physics and Astronomy, UCL, London, WC1E 6BT, UK

10 Institute of Radiophysics and Electronics, NAS of Ukraine, 12 Proskura St., 61085, Kharkov, Ukraine.

11 School of Physics and Astronomy, North Haugh, St Andrews, Fife KY16 9SS, UK

### **Abstract**

The ESA Planck satellite will study the anisotropies of the Cosmic Microwave Background radiation (CMB) over the whole sky with unprecedented sensitivity and high angular resolution. The High Frequency Instrument, HFI, on Planck will observe simultaneously in six bands in the range 100 GHz to 857 GHz. The inclusion of non-CMB bands will allow for the robust removal of foreground sources from the data. This paper is concerned with the design, modeling and predicted performances of the two highest frequency channels centered on 545 GHz and 857 GHz, dedicated to observing these foregrounds and using specialized multi-mode feedhorns. Multi-mode systems have the advantage of increasing the throughput, and thus sensitivity, of the detection assembly when diffraction limited resolution is not required. The horns are configured in a back-to-back setup which transmits the signal through filters to a detector horn. The modeling of the broadband beam patterns on the sky is shown to require careful analysis. Simulations of the complex interactions of the horns is computationally challenging when the detector horn in the relay system is included. The paper describes the approach to modeling these high frequency channels and discusses how the optical requirements on the horn designs are met in terms of spillover, edge taper, illumination of the telescope aperture and beam patterns on the sky.

### **1 INTRODUCTION**

The primary objective of the Planck mission (Tauber 2009a & 2009b) is to study the Cosmic Microwave Background (CMB) with the unprecedented sensitivity possible from deep space. The extended frequency coverage of the two instruments on board Planck (the Low Frequency Instrument or LFI (Bersanelli 2009) and High Frequency Instrument or HFI, Lamarre 2009) will also improve our understanding of far-infrared foregrounds both extragalactic sources and the gas and dust of our own galaxy. This is important for achieving the ultimate sensitivity because Planck's measurement noise on the CMB is lower than the level of contamination expected from the foregrounds, even in clean regions of the sky.

This paper is specifically concerned with the design and predicted performances of the two highest frequency channels of the HFI which use specialized multi-mode feedhorns (Murphy 2001, Colgan 2001, Gleeson 2004, Noviello 2008) and are dedicated to observing these foregrounds. For these two high frequency multi-mode bands centred on 545 GHz and 857 GHz (each with a 30% bandwidth)

the telescope is the main source of thermal radiation and photon noise and the design of these horns require a very special approach.

The HFI bolometers (Bock 1995) are incoherent detectors and thus absorb the total power in the propagating modes transmitted by the feed systems which optically couple the detectors through corrugated waveguide structures to an off-axis Gregorian telescope (Tauber 2009a). The telescope primary mirror has a projected diameter of 1.5m which provides a diffraction limited resolution of the order 2-3 arcmins for the two bands at 545 GHz and 857 GHz. There is a requirement to maintain a beam width close to 5 arcmins to minimize the number of positional changes of the satellite and to keep the data rate within the available downlink specification. That allows a multi-mode detection scheme to be implemented, making use of partially coherent optics (Withington 1998) based on the use of scalar feedhorns (Maffei 2000) fed by an overmode waveguide.

The multi-mode design adopted for these two channels has the goal of maximizing the response to point sources while keeping the beam size large enough (4-5 arcmins) to meet the sampling requirements. In the multi-mode horns the waveguide section is oversized for the wavelength range selected by quasi-optically coupled mesh filters (Ade 2009), giving an effective throughput greater than for a diffraction limited system. The multi-mode channels are unique in their design and function and their development has necessitated the extension of existing modeling techniques including the analysis of overmode corrugated waveguides (Clarricoats 1984, Murphy 2001, Gleeson 2005) and the propagation of partially coherent fields through the telescope optics and onto the sky (Yurchenko 2001 & 2004, Brossard 2001, Noviello 2008). The shaped horn configuration maintains control of sidelobes and modifies the partially coherent illumination of the telescope (Maffei 2000). The technique has the advantage of increasing the throughput and thus sensitivity of the detection assembly, each extra mode contributing to the power detected. The drawback is the resulting beam characteristics are significantly more complicated to model and the boundary conditions are not as accurately controlled as for the single-mode channels because the precise balance of power in the modes is affected by the details of the feed relay system, which has the potential for cavity effects (Ade 2009, Maffei 2009).

A previous paper on the focal plane configuration has been devoted to the design optimization and beam performances of Planck-HFI concentrating mainly on the CMB single mode channels (Maffei 2009). This paper is dedicated to a detailed description of the design and modeling of the multi-mode channels of the HFI, ultimately focusing on beam pattern prediction for the channels at 545 GHz and 857 GHz, and the throughput of the horns. In section 2 we will describe the design solutions adopted to reach the specifications including the requirements on illumination pattern of the telescope, edge taper and spillover levels. In section 3 we discuss the computational approach taken for the modeling of the multi-mode horns, while in Section 4 we describe how the horns reach the requirements in terms of telescope illumination and phase centre location and we also discuss the comparison with the laboratory test measurements of the Planck pixel configuration. Section 5 is dedicated to the extensive telescope beam simulations performed for the multi-mode channels based on the best expected performances of the horns and knowledge of the real in-flight telescope.

## **2 OPTICAL CONSIDERATIONS & DESIGN CONSTRAINTS**

The Planck-HFI detection system is based on cryogenically cooled ultra sensitive bolometers (Bock 1995) coupled to corrugated feedhorn antennas directly illuminating the telescope secondary mirror (Tauber 2009a). Shaped corrugated feedhorns have been chosen for all channels to achieve very low sidelobe levels and strict stray-light control (Maffei 2000) demanded by the stringent requirements for the CMB measurements, but also necessary for high sensitivity foreground observations (Lamarre 2003). There are no quasi-optical components in front of the horn aperture (as for example

in the QUAD experiment (O'Sullivan 2008)) which would have resulted in main beam distortion and necessitated a cold stop to terminate an overall increase in sidelobe levels. Instead the front horn is part of a triple horn configuration in which the filters are located in between a back-to-back (BTB) horn and the detector horn (see Fig. 1, Ade 2009). All of the waveguide sections are corrugated and act as high pass filters defining the lower edge of the bands for the CMB channels (Gleeson 2005). The design principle behind the triple horn configuration forming the detection assembly is presented in detail in Ade *et al.*, (2009) and is based on a design concept by Church (1996). This arrangement is ideal for the single-mode CMB channels in that the optically coupled mesh filters will have no impact on the horn beam patterns. However for the multi-mode channels the components after that BTB waveguide can influence the detailed structure of the patterns which needs to be considered and analyzed.

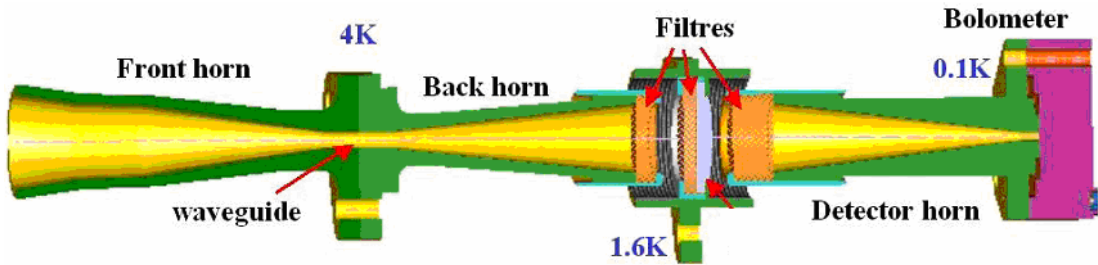


**Fig. 1.** The typical optical chain for the HFI channels is shown schematically. The front horn determines the light collected from the telescope. It also strongly limits the sidelobe levels in the pattern illuminating the telescope reflectors. Its wave-guide section determines which modes couple to the detector. The back horn launches the radiation through a set of filters into the 100 mK horn that concentrates it onto the bolometer in the detector cavity.

Planck has a diffraction limit of a few arc mins in the highest frequency bands (centered on 545 GHz and 857 GHz and with a 30% bandwidth), yielding a higher resolution than the required 5 arcmins. The use of multi-mode optics allows us to take advantage of increased sensitivity of the detection assembly over the diffraction limit. However, the multi-mode horn beams are theoretically more complicated to model in the complex Planck pixel design and actually less predictable in their actual performance than single-mode channels because of the propagation, scattering and potential reflections of multiple modes in the triple horn and cavity configuration. Nevertheless, the extra propagating modes in a multi-mode design improve the illumination pattern of the antenna, increasing the throughput and hence instantaneous directivity. Note that the optical definition of the low frequency side of the 545 and 857 GHz photometric bands is achieved using metal mesh filters (Ade 2009) rather than being defined by the cut-off of the fundamental corrugated waveguide mode as in the case of the single mode horns (Maffei 2000 & 2009, Gleeson 2005).

Clearly we need to be sensitive to faint foreground sources and so it is crucial to reduce unwanted signals to a minimum. Thus, the reduction of the spillover and the maximization of the power concentrated in the horn main beam are of high importance. Since the horns directly illuminate the telescope the horn beam sidelobes have to be minimized, while the main beam fills as much of the telescope aperture as possible. In order to be consistent with the science requirements, it was decided that the spillover has to be maintained to within 1% (Lamarre 2009). At the same time in order to prevent sidelobes due to truncation at the telescope mirrors the edge taper should be around -30dB. The design therefore needs to balance increased throughput and instantaneous sensitivity to a point source while simultaneously meeting the spillover and edge taper requirements.

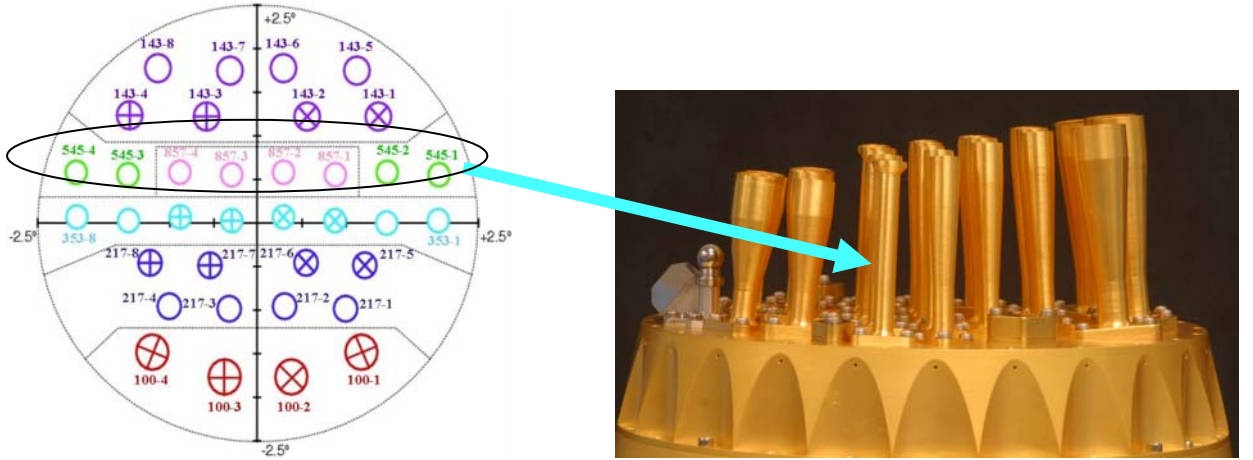


**Fig. 2.** Focal plane layout of the HFI horns. The 545 and 857 GHz horns are positioned where the optical quality is good enough for high frequencies. The curvature of rows compensates for the distortion of images by the telescope. The horns are designed so there is no shadowing by adjacent rows.

Assuming that we are observing a source with a brightness distribution  $B_\nu(\Omega)$  the power received by a detector (Maffei 2009) is:

$$P = \int_{\Delta} A\Omega \varepsilon(\nu) B_\nu(\Omega) d\nu d\Omega$$

$\Delta$  is the spectral bandwidth of the channel. The throughput is  $A\Omega = n(\lambda)\lambda^2$ , where ideally  $n(\lambda)$  is the number of modes at wavelength  $\lambda$  that optimizes the horn beam illumination of the telescope while meeting the spillover/edge taper requirements and giving a beam on the sky of the required resolution.  $A$  is the effective aperture area of either the horn or telescope, and  $\Omega$  the corresponding horn or telescope beam solid angle.  $n(\lambda)$  can be adjusted to optimize throughput using the filtering effect of the waveguide.  $\varepsilon(\nu)$  is the optical efficiency and includes the detector efficiency term,  $\eta$ , set by the detector design and manufacture. One of the major tasks was to optimize the optical efficiency as described in Maffei (2009).

Coupling the horn directly to the telescope defines the optical characteristics of the instrument (resolution, the antenna beam shape (main beam and part of the sidelobe structure) and the spillover). For the high frequency multi-mode horns the balance between the modes propagating through the waveguide filter into the front horn determines the beam illuminating the telescope and thus the resolution, spillover and edge taper. This balance depends ultimately on how these modes couple to the detector which is not necessarily a well controlled process. In modeling horns we have assumed optimal coupling to the bolometer as likely to be close to operational reality (Maffei 2009).

Apart from the horn aperture and waveguide being determined by the optical requirements there are also some mechanical limitations on the horn design as a result of their position at the centre of an array of the larger horn antennas for the longer wavelength channels (see Fig 2). Each front horn has also been designed such that its phase centre is located on the telescope focal surface. The off-axis Gregorian telescope configuration (compensated aplanatic design to optimize the required field of view to accommodate the large focal plane assembly (Tauber 2009a)) results in a focal surface with an off-centre apex. This shape has a pronounced slope across the focal surface. The high frequency horns are located in a line close to the centre of the focal surface where aberrational losses are least severe for the extended field of view. At this location the length of the high frequency horns was significantly influenced by the need to prevent shadowing by adjacent horns on the sloped focal

surface (see Fig. 2). This implies tapered horns long for the operating wavelength band which turned out to be challenging to manufacture. The phase centre (determining location relative to the focal plane) was required to be within 4 mm of the horn aperture (Gleeson 2002), see Fig. 3.

Manufacturing consideration forced modification of the original tapered horn profile of the back-to-back (BTB) section (as illustrated in Fig. 3 below), resulting in a more abrupt profile for the horn adjacent to the waveguide filter section. This has the potential to reduce somewhat the performance of the horn beam by increasing reflections from this part of the horn. A similar design was used for the detector horn. This effect was carefully analyzed to ensure no deterioration in multi-mode operation in terms of beam pattern, and throughput. In fact the beam patterns still achieve close to the desired requirements for sidelobe levels although the main beam is less top-hat like (and thus the illumination pattern is somewhat less ideal, increasing the beamwidth marginally) and there are some more significant cavity effects due to the reflections in the system.

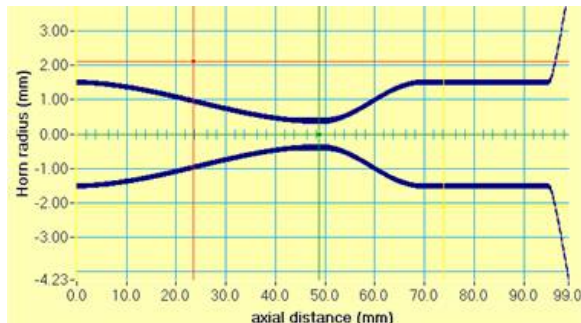


**Fig 3 (a)** Profiled flare-original concept

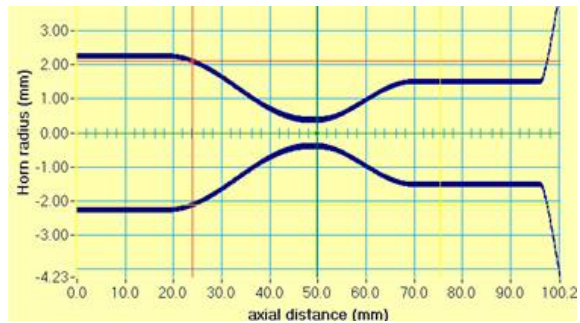


**Fig 3 (b)** Final manufactureable design

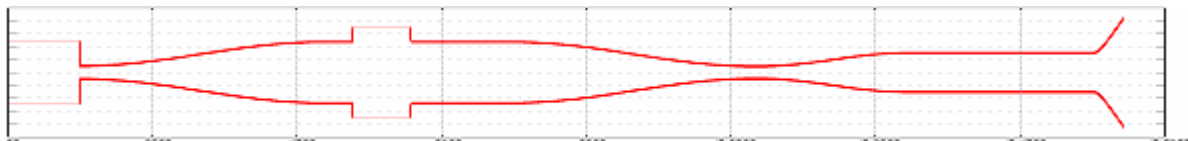


**Fig 3 (c)** Schematic diagram of horn profile for full pixel simulations (vertical scale exaggerated)

### 3 MODELING OF THE MULTI- HORNS

In the high frequency 545 GHz and 857 GHz Planck pixels both the back-to-back (BTB) horn and the detector horn have overmode waveguide filters (see Fig 4). We can model the waveguide-horn structures using the same scattering matrix approach used for the single-mode-CMB-channel horns (Maffei 2000) except we include modes of all azimuthal orders  $n$  that can propagate, not just those with  $n = 1$  (Murphy 2001, Colgan 2001, Gleeson 2004, Noviello 2008). In terms of the beam patterns we assume reciprocity and that the cavity behaves like a black-body. Thus, all waveguide modes are equally excited in power in the effective blackbody cavity in which the bolometer is located, and independently of each other so there is no phase relationship between them. Thus, many of these modes will contribute independently (i.e. incoherently) to the beam on the sky. A single-mode horn transmits only one pair of orthogonal coherent fields, the HE<sub>11</sub> hybrid mode. In a multi-mode horn several independent pairs of orthogonal coherent fields will be present which will need to be propagated through the Planck telescope to predict the beams on the sky.

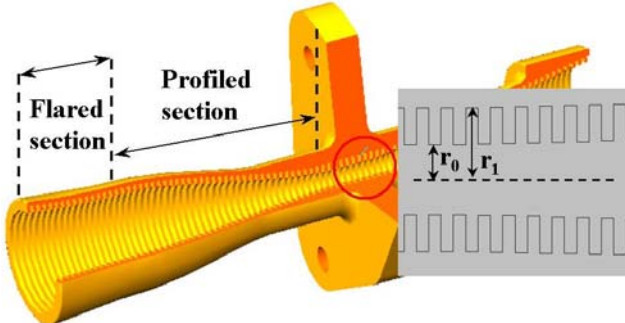


**Fig. 4** Section through horn showing the corrugations. The natural modes of such a system are hybrid waveguide modes (neither TE nor TM). Such corrugated guides can be modeled as cascaded short smooth-wall segments as a band pass filter for hybrid modes.

An important issue is how well modes in the cavity make it through the detector horn waveguide filter relay and couple to the BTB horn. Since the waveguide filter in the detector horn is wider than that of the BTB, it is a reasonable working assumption that any mode that can propagate through the BTB also propagates through the detector horn waveguide from the cavity. Thus, as far as the beam patterns are concerned a useful first order working model is to assume that the BTB is effectively coupled to a black body cavity (i.e. the detector cavity) also. Equivalently, all modes are excited at the back end of the BTB horn independently with equal power. We also investigated models that included the coupling through to the bolometer cavity via the detector horn. This resulted in a better understanding of the behaviour of the system across the band and is detailed in section 5.

If there are a sufficient number of corrugations per wavelength the walls of the waveguide or horn can mimic a smooth continuous surface with a non-isotropic impedance. According to (Clarricoats 1984) four corrugations per free space wavelength are usually sufficient for this assumption. The natural propagating modes of such waveguides are known as the hybrid modes referred to above (pure transverse electric (TE) or transverse magnetic (TM) modal fields are not allowed). A circular corrugated waveguide is described by its radius and by the depth of the corrugations giving two parameters  $r_0$  and  $r_1$  (see Fig 4). Within the context of the hybrid mode model these two radii will define the high frequency and low frequency cut-offs of the modes that can propagate in any waveguide section forming a bandpass filter for each mode. Only a limited number of hybrid modes

can propagate at any one frequency. The actual band of frequencies that can be transmitted is defined by the interference mesh filter stack (Ade 2009) located between the BTB and detector horns. Thus in this approximation the single-mode CMB horns carry just the fundamental  $HE_{11}$  hybrid mode whereas in the multi mode corrugated horn antennas considered in this paper, the waveguide filter section is designed to allow several hybrid modes to propagate (Gleeson 2005). Note that different modes cut-on and cut-off at various frequencies across the photometric band. Thus at a single frequency only a subset of these modes will propagate. This approach gives a good understanding of the operation of the filter although it turns out to be awkward for the shaped horn where the relatively abrupt profiles results in significant mode scattering of these hybrid modes.

We can choose any complete set of modes to represent the black body field at the back aperture of the BTB (the aperture facing the detector horn where the band pass filters are located). Since corrugated waveguide modes are essentially hybrid (coherent mixtures of TE and TM modal fields), and not applicable when modeling the profiled horn shape, we take a mode scattering approach and use *smooth-wall* waveguide modes. In this picture the corrugated guide is considered to be a sequence of very short smooth-wall guide sections (representing sequentially the corrugation grooves and fins), with clearly significant scattering of these smooth-wall waveguide modes occurring at *each* corrugation step (Olver 1994). Thus, for each horn segment the natural modes of propagation are the usual  $TE_{nl}$  and  $TM_{nl}$  modes of a cylindrical waveguide (Murphy 2001, Colgan 2001, Gleeson 2004, Noviello 2008), with two possible orthogonal  $TE_{nl}$  and  $TM_{nl}$  fields for  $n > 0$  because of the cylindrical symmetry. At the junction between two segments the scattering of power between modes occurs which is kept track of using a mode matching technique such that complex power is conserved. By computing the scattering matrix terms for each junction we can compute the cascaded scattering matrix for the complete shaped waveguide horn structures. This has been shown to predict the beam patterns of single-mode horns to high accuracy and reproducibility (Maffei 2001).

The details of the electromagnetic theory of multi-mode horn operation using this scattering matrix approach is given in a number of publications (Murphy 2001, Colgan 2001, Gleeson 2004, Noviello 2008). On propagation the family of modes with the same azimuthal symmetry scatter power into each other, but not to modes with a different azimuthal order  $n$ , which simplifies the computation significantly. Also only modes up to a certain azimuthal order can propagate through the waveguide filter due to smooth-wall waveguide cut-off effects. Because of the significant modal scattering there is also some reflection of the power in the smooth-wall-waveguide modes at the entrance to the BTB horn, even for those modes that are not cut-off in the filter.

Clearly in this discussion the term “mode” can be ambiguous, whether used within the context of the hybrid mode model or the mode matching scattering matrix technique with smooth-wall waveguide modes as the “basis” set of fields. The hybrid mode assumption is valid if there are several corrugations per wavelength and if there is no abrupt change in the waveguide profile. Within this framework, each hybrid mode propagating in the horn is considered as a combination of smooth-wall *TE* and *TM* scattering matrix modes (Gleeson 2004 and Noviello 2008). The scattering matrix approach however is more accurate, particularly so as the number of corrugations per wavelength is lower than ideal for the high frequency 857 GHz channels because of manufacturing limitations. At 990 GHz, the top end of the band, for example, there are only two corrugations per wavelength. Furthermore the shaped horns give rise to significant mode scattering even in the case of hybrid modes. Many of these smooth-wall *TE* and *TM* waveguide mode fields at the input, when propagated to the BTB, produce horn aperture fields that are not linearly independent but rather are mixtures of smaller numbers of true hybrid modes (which can in theory be extracted).

Based on a previous geometry (del Rio 1999) a profiled-flared shaped horn (Fig. 4) has been developed for Planck (Maffei 2000) and also used for the earlier experiment Archeops (a CMB experiment to test the Planck concept (Benoit 2002)) to produce the required beam shape. The carefully optimized hyperbolic flare section reduces the sidelobes surrounding the main beam to acceptable levels (the flare length chosen was a compromise between optimized sidelobe reduction, beam illumination pattern and the necessity to place the horn phase centre close to the horn aperture). Note that while the phase centre of a profiled horn is located close to its aperture, the addition of the hyperbolic flare moves it further inside the new aperture, the precise location depending on the length and the tilt of this flare and the frequency. This effect had to be taken into account when designing the horns in order that these meet all the optical requirements and thus were at the correct location with respect to the focal surface to not shadow, or be shadowed by, the other horns.

At the front aperture of the BTB we can recover the true independent hybrid fields that are transmitted by the waveguide filter and horn. These hybrid fields propagate independently through the telescope and onto the sky since they were generated by an independent set of smooth-wall waveguide modes at the effective black body enclosure at the back aperture of the BTB. (Olver 1994, Maffei 2000)

The columns of the  $S_{21}$  scattering matrix contain the mode coefficients for the modal sums required to recover the independent hybrid fields at the horn aperture. These fields, once recovered, must be propagated to the sky independently and then be added in quadrature to simulate a true multi-mode beam pattern, each simulation being at a single frequency. In order to produce a true beam pattern for the band these single frequency fields must be added in quadrature across the band with any non-uniform weighting to take into account any non-uniform transmission for the filters that define the band. The spectrum of the source will also affect the beam pattern for any particular observation.

All the back-to-back high frequency horns of HFI went through qualification and characterization tests at single component level. The result of their transmission measurements is reported in another publication (Maffei 2009), which includes beam pattern measurements outside of the normal operating band at a frequency at which the horns were single-mode. The horns show very little deviation from the ideal pattern (model prediction for single mode operation) at the level of their main beam (+/- 25deg corresponding to the edge taper) indicating the absence of obvious manufacturing defects likely to affect the beam patterns. The measurements of the beam patterns made at multi-mode operation is discussed below in section 4.

#### **4. FAR-FIELD PATTERNS OF HORN AND LABORATORY TESTS**

##### **Telescope Illumination Patterns**

The simulated broadband far-field patterns of the 545 and 857 GHz horns are shown in Fig. 5 below. In Figs. 5a & b we assume black-body illumination of the front BTB horns, equivalent to assuming perfect coupling through the relay feed system to the detector. A more realistic simplified model of the full Planck pixel, including the detector horn and transition to the bolometer cavity, has also been investigated (see section 5). The beams for the 857 GHz horn are shown in Fig. 5a at spot frequencies at the band edges (730GHz and 990GHz) and centre (857 GHz) illustrating that the beam width remains approximately constant (throughput conservation). Similarly, the 545 GHz horn beams are shown at the band centre and the edges (Fig 5b).

Two assumptions were made here in modeling the full pixel (BTB plus detector horn): (i) the filter section could be described by a smooth waveguide section of the same diameter as the mesh filters

and (ii) the bolometer cavity itself is approximated as a radiating black body source or sink (no reflections)- see Fig 3c. An exact representation of the pixel was not possible because of the nature of the quasi-optical coupling of the filter section. To overcome this difficulty a number of example cases were considered, in which further simulations were undertaken, to quantify the effects on the beam patterns of the BTB resulting from inclusion of the cavity, detector horn and the filter-assembly in the analysis. With the help of these varied theoretical techniques, in-flight performance can be estimated (see later in this section for further discussion).

Comparison of the plots shows that the detector horn and filter section act as a good relay for coupling to the BTB horn so that the assumption of blackbody illumination of the front BTB horn would appear to be valid. Note that the edge tapers in all cases satisfy the requirement of better than -30dB at 26 degrees at the centre of the band. The spillover values for the various horns are given in table 1.

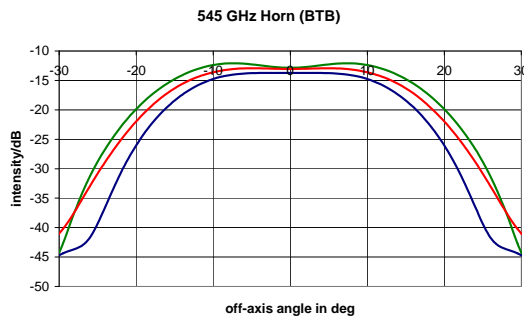


**Fig. 5a** Comparison 545 BTB far-field horn beam patterns at band centre and band edges. (Green-465, Red-545 GHz, Blue-625 GHz)

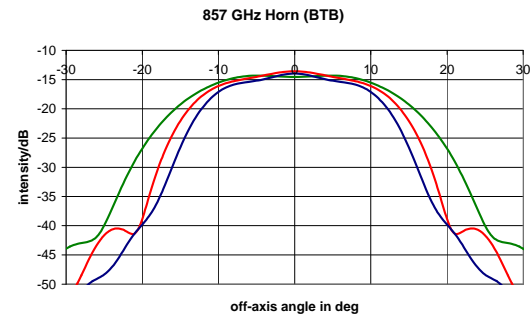


**Fig. 5b** Comparison 857 BTB far-field horn beam patterns at band centre and band edges. (730 Green-730 GHz, Red- 857 GHz, Blue-990 GHz)

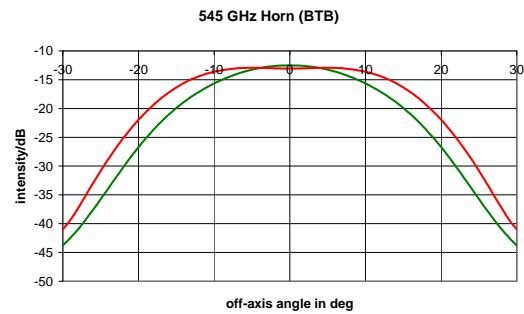


**Fig. 5c** Comparison of far-field horn beam patterns at band centre for 545 GHz horn for BTB (red) and full pixel cases (green).

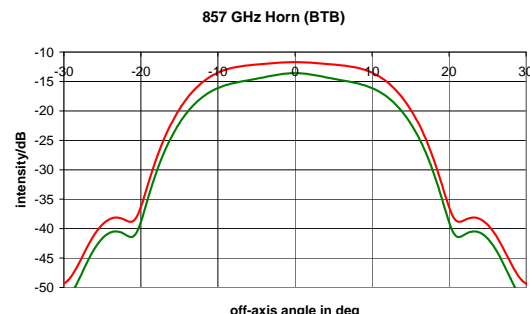


**Fig. 5d** Comparison of far-field horn beam patterns at band centre for 857 GHz horn for BTB (red) and full pixel cases (green).

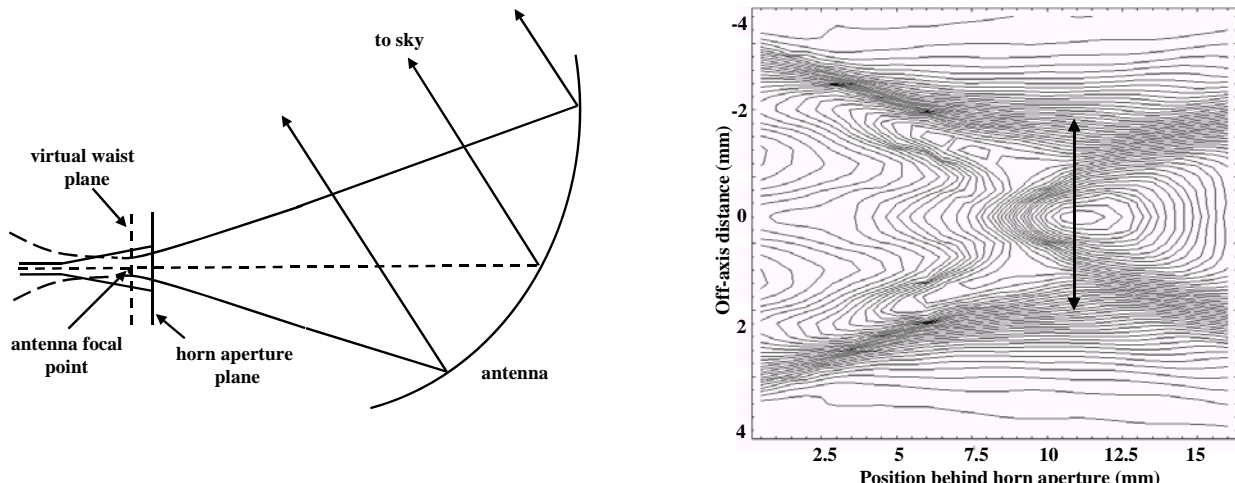
Spillover and edge-taper levels		
Average Values	545 GHz	857 GHz
Spillover (26 deg)	0.0056	0.0011
Edge Taper (26 deg)	-26.0 dB	-29 dB

Table 1: Spillover and edge-taper levels

## Horn Phase Centres

Determining the so called phase-centres of multi-mode horns requires careful consideration. The “phase center” is ill defined as the individual spatially coherent fields making up the far-field pattern all appear to come from different phase center locations inside the horn aperture. The best location at which to place these horns with respect to the focal surface therefore requires a different approach from that of a single mode horn (Maffei 2000). In this case it is reasonable that the average phase center location is best defined in terms of the virtual beam waist position behind the horn aperture. The focus of the telescope should be located at this waist in order to optimize the angular resolution and on-axis gain for the beam on the sky (Gleeson 2002). However, because of the multimode nature of the beam, the position where the on-axis gain is a maximum may not coincide precisely with the optimized angular resolution.

Since the phase front of the horn aperture is convex, the effective phase center will be located inside the horn. We can locate this virtual waist (for the band centre) by propagating the horn aperture fields backwards into virtual space behind the horn aperture plane and determine the position at which the beam appears narrowest (see Fig. 6). The individual spatially coherent component fields must be propagated separately and combined in quadrature to determine the intensity pattern. The waist position is also frequency dependent.



**Fig. 6.** Schematic of set-up of a horn aperture with respect to an antenna illustrating the horn virtual waist and antenna focal point. Typical behaviour of the beam in the vicinity of the virtual waist location is also illustrated.

The effects of telescope truncation can be neglected in determining the position of the best phase center as, in Planck, the beam edge tapers at the telescope are very low (about  $-30\text{dB}$ ) and to a good approximation the telescope can be assumed to be of infinite extent. Thus the field on the sky will be an image of the horn field at the telescope focus without much broadening because of the low level of spatial filtering at the telescope aperture. Aberrations degrade the resolution slightly.

The *depth-of-field* will be affected by the spatial filtering of the telescope. A realistic estimate for these horns is obtained by including the effects of the edge taper at the telescope, which thus involves coupling the far-field of the horn to the telescope and defocusing the

system by adjusting the distance between the horn and telescope, effectively changing the phase curvature of the beam at the telescope aperture. Replacing the telescope with an equivalent paraboloid, the radiation pattern on the sky is obtained by summing in quadrature the Fourier transforms of the far-fields of the independent spatial modes of the horn with the appropriate phase error across the telescope aperture. In this case we can then analyze the variation of the on-axis gain on the sky with defocus distance as a convenient parameter for checking the depth of field on the focal plane.

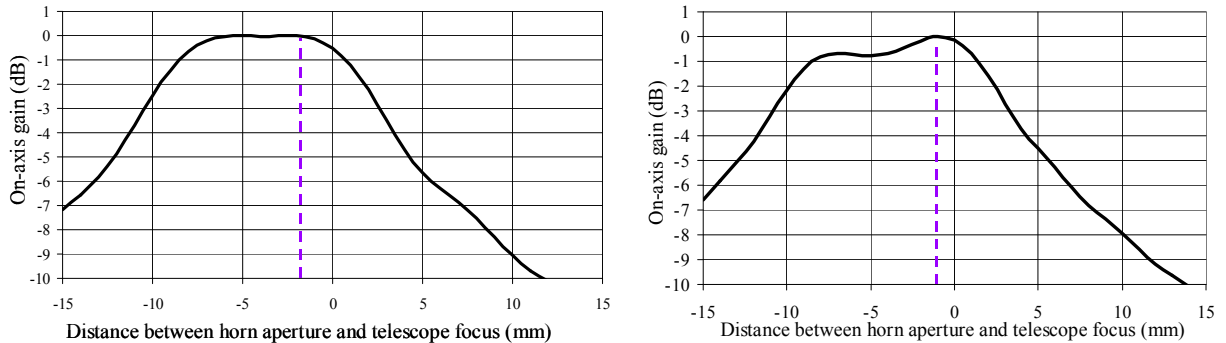


**Fig. 7** Broadband on-axis gain in the far-field of a perfect telescope for varying displacements of the horn aperture with respect to the telescope focus for the 545 GHz (left) and 857 GHz (right) horns. Optimum gain lies between 2 mm and 7 mm behind the horn aperture.

Fig. 7 shows the broadband on-axis gain of the horn with horn aperture displacement away from the focal plane. A negative distance implies that the focus is positioned behind the aperture (where it is expected). The maximum on-axis gain occurs when the telescope focus lies approximately 2 mm behind the horn aperture, thus satisfying the Planck requirement that the phase centre must be no more than 4 mm from the aperture to prevent shadowing of other horns in the HFI and LFI arrays. For both horns the depth of field (whose edge is defined by the 1dB below the peak level) is about 10 mm in both cases indicating a rather tolerant system to axial positional inaccuracies and satisfying all phase centre requirements.

### Test Measurements

The special operation in space of the multi-mode Planck pixels with unimpeded illumination of the telescope and low temperature of the optical elements meant that an exact measurement of the optical response could not be made under flight conditions. Instead on-ground characterization of these pixels has been based on multiple measurements of qualification and flight model feed-horns. The operation of overmoded BTB horns has also been investigated using scaled prototypes (Gleeson 2004) to verify theoretical techniques for modeling such horn systems. The flight model BTB horns were tested for single mode operation at a frequency below the actual band of operation to check for manufacture defects. Under single mode operation the beam is unaffected by the part of the pixel behind the BTB waveguide filter.

Measurements were made at Cardiff University of a full pixel at 857 GHz in a similar arrangement to the actual flight configuration, although it was necessary to place a cryostat window behind the BTB horn, and to introduce an extra relay BTB horn section (Ade & Savini 2009). The 857 GHz full pixel broadband beams that were measured are narrower than those predicted by the simulations (see Fig. 8). The figure shows the results of the measurements made over the band defined by the Planck filters. Shown also are spot frequency measurements also made with a narrowband coherent source (backward wave oscillator) again superimposed on the simulations. The horns are clearly working in a multimode fashion and it is possible to show that the partially coherent fields can be re-expressed

as a sum of hybrid fields. The discrepancies are understandable when the measurement set-up is considered, particularly the necessity to include an extra BTB relay horn which leads to extra mode filtering. The analysis of this system is considered in detail in Ade & Savini (2009).

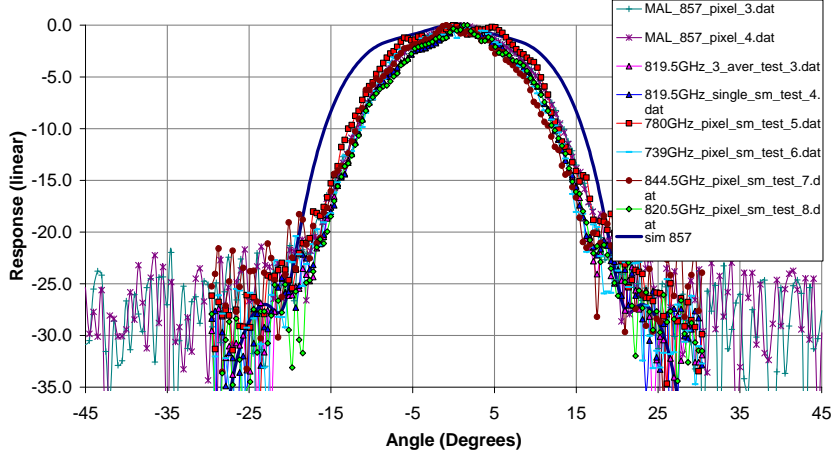


**Fig. 8:** Horn far-field measurements were made at Cardiff for broadband and spot frequencies with the BTB horn both outside and inside the test Dewar window (the inside case is more challenging but more representative of the true Planck pixel).

When we compare the idealized model at a frequency of 857 GHz with the spot frequency measurements across the band the theoretical beams appear to be too wide, indicating missing modes in the measured beam. We group contributions according to azimuthal order and overlay with the measurement data to investigate which field distributions are missing. Modes of order 2 and higher appear to be absent. If we only add modes of azimuthal order  $n = 0$  and 1 together the resulting beam pattern prediction appears to fit the measured beams to a reasonable approximation (see Fig. 9). This suggests a loss in throughput, as if we assume  $A\Omega = n\lambda^2$ , then  $\Omega_{\text{meas}} / \Omega_{\text{sim}} = n_{\text{meas}} / n_{\text{sim}}$ , giving a 20% to 30% loss in measured beam area, corresponding to a 20%/30% loss in the number of modes. In the case of the in-flight behaviour of the Planck pixel however we expect to have beam patterns that have wider beams than suggested by the measurements as modeling of the full pixel indicates no significant attenuation of the modes making up the multi-mode distribution over the BTB.

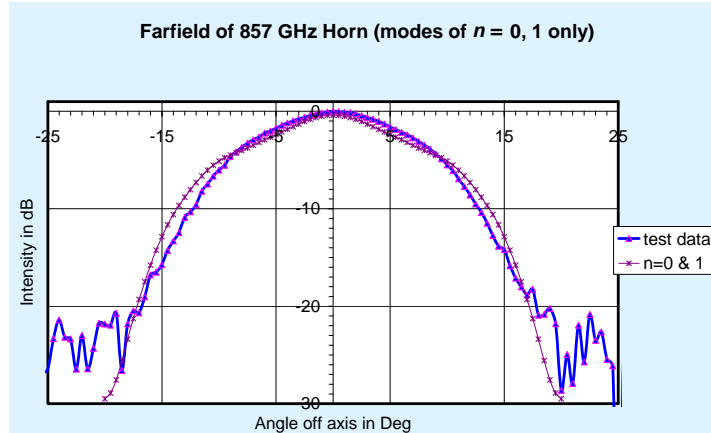


**Fig. 9:** Test data fitted with beam with reduced mode content at the band centre.

## Discussion: Simulation of the realistic horn beams

Realistic beam patterns on the sky require realistic models of the horns. The simulation of the full horn assemblies themselves has been a revealing and challenging undertaking, particularly when including the coupling to the detector horn in the simulations. To perform these simulations of the multi-horns it has been necessary to develop a computationally efficient modeling program. The code performs run-time checks on the numerical stability of the scattering model at each junction and basic checks on the physical plausibility of the model. With the new software the pixel assembly could be simulated in 1GHz steps across the band for a number of models. This has been done for the ideal (as designed) horn and, in the case of the 545 GHz horn, for eight models of horns with manufacturing tolerances not exceeding  $2\mu\text{m}$  applied on a section-by-section basis to see if there was any observable effect. For the 857 GHz horn the effect of manufacturing tolerances has been examined for eleven models at a number of spot frequencies.

The more realistic models presume a perfect filter in front of the detector horn, and the working assumption is that the bolometer cavity is a perfect black body across the band. The horn models do not take into account assembly imperfections that would result in imperfect alignment of the sections. Misalignment would give rise to the exchange of power between fields of different orders, effectively giving rise to leakage of power into non-propagating fields. It is not immediately obvious what the effect of misalignment would be, but it would probably result in a very small reduction in throughput and some damping of any power trapped due standing waves in the system.

Overall the performance of the complete horn assemblies is similar to that of the back-to-back horn alone, with a reduced throughput, but a similar change in beam pattern across the band. The modelling indicates that there is trapped power between the bolometer horn and the back-to-back horn, the horn configuration acting as a leaky cavity (see Fig. 1). This gives rise to rapid frequency dependent changes in throughput. Furthermore, as well as total power transmission variations, there is frequency dependent variation in the distribution of power between fields of all orders. That means that there are the beam pattern changes with frequency that would not occur in the BTB horn. Because it is not possible to know what has been built to the level of accuracy to which the horn is sensitive, it is not possible to know precisely what the beam pattern will be in very narrow bands. Nevertheless, over any reasonable band this 'ringing' tends to average out, and the net effect is only a reduction in throughput.

Inclusion of damping due to finite conductivity does not materially effect the qualitative behaviour observed. Single frequency or very narrow-band beam pattern prediction should be considered only as a qualitative indicator of performance. This is because very small manufacturing tolerances change the distribution of power between transmitted fields in much the same way as a change in frequency. As a result, the qualitative behaviour of two tolerance models of the broadband horn will be much the same, but the distribution of power between modes and the mode-by-mode transmission of the different horns will be different at any one frequency.

Conclusions made above are also supported by the analysis of lower frequency HFI horns comparison of the HFI 100GHz BTB horns. However, with an approximate model of the full 100 GHz pixel assembly only very weak 'ringing' is seen with almost unity power transmission across the band dropping off sharply below 86GHz.

## **5. TELESCOPE MAIN BEAM PATTERN SIMULATIONS USING GRASP**

Since the detectors are rather wideband and the GRASP calculations are monochromatic, several spot frequency patterns need to be calculated and averaged to simulate the beam pattern, with each calculation repeated for each orthogonal polarization. For each main beam single polarization characterization several frequencies were calculated across the band. For multi-mode horns the number of modes transmitted to the bolometer varies with the frequency. The resulting fields are incoherent sums of all the modes present and the beam pattern varies with frequency. Analysis of the scattering models of the 857 GHz horn aperture fields indicates that there are essentially only a small number of independent hybrid mode fields contributing to the beam on the sky. Modeling the telescope beams involves identifying those hybrid aperture fields which have significant power and independently propagating them through the telescope one at a time for spot frequencies across the band, then adding in quadrature.

The broad-band beam for the 857 GHz horn was modelled between 730 GHz and 990 GHz in 5 GHz steps; a total of 53 frequencies (see Figs 10 & 11). The model of the horn used 64 modes in each azimuthal order 0 through to 4; there is no transmitted power in higher azimuthal orders. Thus, at each frequency the horn model has an input of 320 waveguide modes of unit amplitude, the output being a frequency dependent number of aperture fields. In all, 743 aperture fields were found to be sufficient for a good description of the broad-band beam. Each of these fields is coherent and has to be propagated independently through the telescope model to the sky. Having calculated the beam pattern on the sky for each aperture field they are summed in quadrature. This process gives a broad-band beam power density pattern with units W/sr (the units used by GRASP for far-fields).

The 545GHz pixel broad-band telescope beam has been simulated taking the same approach as that described for the 857 GHz pixel. The beam pattern described below is derived from 64 single frequency contributions (see Figs 10 & 11).

Note that since the main beam will not be Gaussian, being made up of many modes, a classic Full Width Half Maximum (FWHM) used on a typical quasi-Gaussian main beam becomes an inappropriate measure of the beam width. Examples of such beams are shown in Figs. 10 and Fig 11 for the full pixel detection assemblies computed across the spectral bandwidth (broadband). The main beam is clearly non-Gaussian and the usual value of the FWHM becomes very sensitive to on-axis gain. A better definition is the Half Power Beam Width (HPBW) in these cases defined to be the radius of a circle including one half of the total power in the beam.

Estimates for the FWHM and HPBW are obtained by taking two beam cuts through the centroid of the unweighted beams in the widest and narrowest directions. For the H-857-1 pixel the beam is slightly elliptical and rotated through approximately 30 degrees. The estimates for the beam without any spectral weighting are: FWHM:  $5.051 \times 4.835$  arc min; HPBW:  $3.668 \times 3.448$  arc min. Fig. 11a shows the two orthogonal cuts through the spectrally unweighted beam. Spectrally weighting the beams for Mars, Sirius, HII regions and cold cores changes the beam pattern so little (except for an overall scaling) that it is not observable on a plot except upon very close examination (see Fig. 10a.). The broad-band beams are therefore not spectrally biased.

The broad-band beam pattern FWHM and HPBW estimates for the pixel H-545-2, frequency range 465 to 630 GHz in steps of 5 GHz are: FWHM:  $4.85 \times 4.69$  arc min. HPBW:  $3.74 \times 3.36$  arc min (see Figs. 10b & 11b)

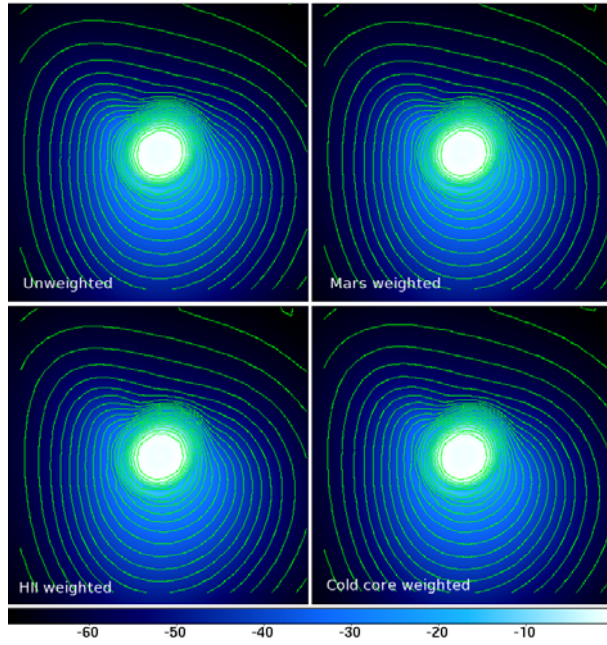


**Fig. 10a.** H-857-1 unweighted and spectrally weighted 730GHz to 990GHz broad band beam patterns. Contour levels are at 3dB intervals. The maps are in Ludwig UV coordinates covering  $30 \times 30$  arc minutes. The differences are discernible in the very low beam levels.

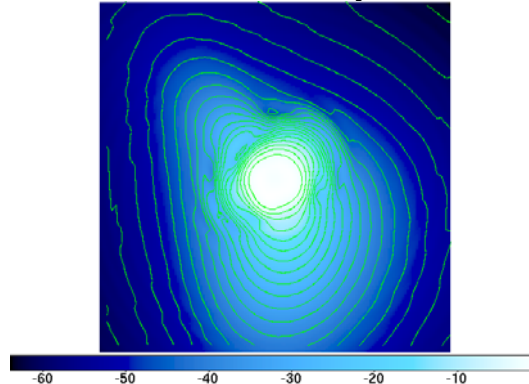


**Fig. 10 b** H-545-2 beam pattern for 465 GHz to 630GHz. Contours are at 3dB intervals. The maps is in Ludwig UV coordinates covering  $30 \times 30$  arc minutes.

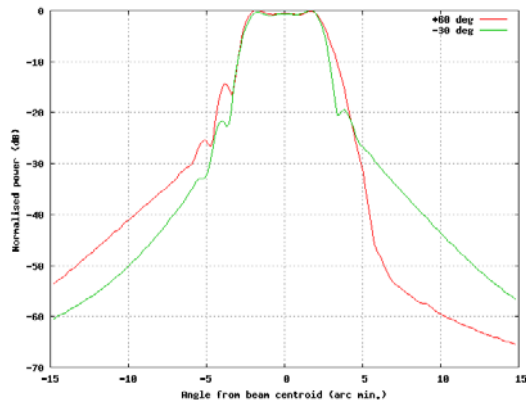


**Fig. 11a** Orthogonal cuts through the H-857-1 beam. (Normalised power in dB.)

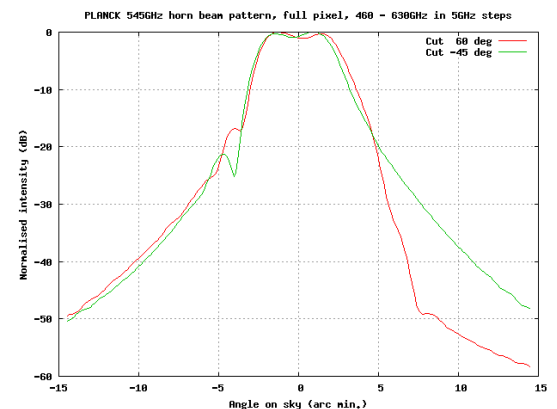


**Fig. 11b** Cuts through the H-545-2 beam. (Normalised power in dB.)

## **DISCUSSION & CONCLUSION**

The *current* best estimates of the beam width for the 850GHz horn indicate that the beam will be close to the design width. This estimate is provisional – the GRASP model uses the best videogrammetry-based estimates of the mirror shapes and the metrology of the telescope assembly to position the mirrors relative to each other, and the final pre-launch beam width estimate has been made taking the focal plane metrology into account in the model.

The modeling of the propagation of the modes inside the optical chain is complex which required the development of novel experimental and theoretical developments. There remain two major unknowns that will determine the beam width on the sky: (i) modal filtering in the flight model horn assembly, and (ii) the coupling of the detector in the cavity to the modes in the horn-waveguide structures. Mode filtering cannot be known until after launch, but damping is probably strong enough to prevent excessively narrow beams. The first observation of planets with the multi-mode channels will give the first accurate measurement of beam size and optical efficiency on point sources.

The current knowledge base provides a good starting point for the in-flight optical calibration activities, which are expected to complement them. The current expectation is that, with the combination of ground knowledge and flight measurements, Planck will be able to achieve its main optical requirements.

## **References**

- Ade, PAR et al. 2009, A & A, this volume.
- Ade P.A.R. & Savini, G. in preparation.
- Benoit, A., Ade, P.A.R., Amblard, A. et al. 2002, Astropart. Phys., 17, 101
- Bersanelli, M., et al. 2009, this issue.
- Bock, JJ et al. 1995, Space Sci. Rev., 74, 229
- Brossard, J. 2001, Ph.D. thesis
- Church, S et al., Proceedings of the 30th ESLAB Symposium on Submillimetre and Far-Infrared Space Instrumentation, ESA-ESTEC, 77, 1996
- Colgan, R. 2001, Electromagnetic and Quasi-Optical Modelling of Horn Antennas for Far-IR Space Applications, Ph.D. thesis, NUI Maynooth
- de Bernardis, P. et al. 2000, Nature, 404, 955
- del Rio Bocio, C., Gonzalo, R., Sorolla Ayza, M. et al. 1999, IEEE Trans. Antennas Propag., 47, 1440
- Gleeson E, Murphy JA, Maffei B, International Journal Of Infrared And Millimeter Waves, 23, 711-730. 2002  
(phase centres)

- Gleeson, E. 2004, Single and Multi- Corrugated Horn Design for Cosmic Microwave Background Experiments, Ph.D. thesis, NUI Maynooth
- Gleeson E, Murphy JA, Maffei B, et al. Infrared Physics & Technology Volume: 46, 493-505, 2005 (Band edge filters)
- Lamarre, J-M et al 2009, The HFI instrument., A & A, this volume.
- Lamarre JM, Puget JL, Bouchet F, et al., New Astronomy Reviews, 47, 1017-1024, 2003.
- Maffei, B et al, 2009, Planck-HFI optical optimization and beam performances
- Maffei, B et al. 2000, Int. J. Infrared and Millimetre waves, 21, 2023-2033, 2000.
- Murphy JA, Colgan R, O'Sullivan C, et al., Infrared Physics & Technology, 42, 515-528. 2001
- Murphy JA, Gleeson E, Cahill G, et al., International Journal Of Infrared And Millimeter Waves, 26, 505-523, 2005
- Noviello, F. 2008, Optical Performance of the ESA Planck Surveyor and Techniques for the Study of the Cosmic Microwave Background, Ph.D. thesis, NUI Maynooth
- O'Sullivan, et al., Infrared Physics & Technology, 51, 277-286. 2008.  
The quasi-optical design of the QUaD telescope
- Tauber, J.A et al. 2009a, The Optical System of Planck, A & A, this volume.
- Tauber, J.A. et al. 2009b, The Planck Mission, A & A, this volume.
- Withington S & Murphy, IEEE Trans Antennas & Propagat, 46, 1651-1659, 1998.
- Yurchenko, V. B., Murphy, J.A. & Lamarre, J.M. et al. 2004, Proceedings of the SPIE, 5487, 542
- Yurchenko, V. B., Murphy, J.A., Lamarre, J.M. et al. 2004, Int. J. Infrared and Millimeter Waves, 25, 601
- Yurchenko, V. B., Murphy, J.A., Lamarre, Int. J. Infrared and Millimeter Waves, 22, 173-184, 2001.